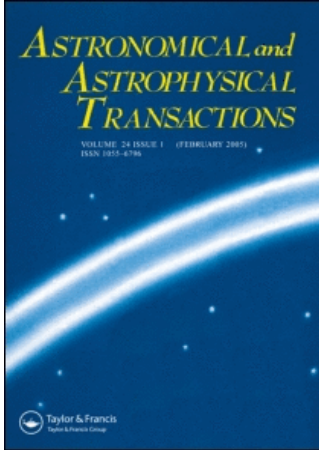


This article was downloaded by:[Bochkarev, N.]
On: 10 December 2007
Access Details: [subscription number 746126554]
Publisher: Taylor & Francis
Informa Ltd Registered in England and Wales Registered Number: 1072954
Registered office: Mortimer House, 37-41 Mortimer Street, London W1T 3JH, UK



Astronomical & Astrophysical Transactions

The Journal of the Eurasian Astronomical Society

Publication details, including instructions for authors and subscription information:
<http://www.informaworld.com/smpp/title~content=t713453505>

Order and chaos of low- and high-energy stars in a galaxy with a strong nuclear bar

N. D. Caranicolas^a; N. J. Papadopoulos^a

^a Department of Physics, Section of Astrophysics, Astronomy and Mechanics, University of Thessaloniki, Thessaloniki, Greece

Online Publication Date: 01 June 2004

To cite this Article: Caranicolas, N. D. and Papadopoulos, N. J. (2004) 'Order and chaos of low- and high-energy stars in a galaxy with a strong nuclear bar', *Astronomical & Astrophysical Transactions*, 23:3, 229 - 239

To link to this article: DOI: 10.1080/10556790410001704659

URL: <http://dx.doi.org/10.1080/10556790410001704659>

PLEASE SCROLL DOWN FOR ARTICLE

Full terms and conditions of use: <http://www.informaworld.com/terms-and-conditions-of-access.pdf>

This article maybe used for research, teaching and private study purposes. Any substantial or systematic reproduction, re-distribution, re-selling, loan or sub-licensing, systematic supply or distribution in any form to anyone is expressly forbidden.

The publisher does not give any warranty express or implied or make any representation that the contents will be complete or accurate or up to date. The accuracy of any instructions, formulae and drug doses should be independently verified with primary sources. The publisher shall not be liable for any loss, actions, claims, proceedings, demand or costs or damages whatsoever or howsoever caused arising directly or indirectly in connection with or arising out of the use of this material.

ORDER AND CHAOS OF LOW- AND HIGH-ENERGY STARS IN A GALAXY WITH A STRONG NUCLEAR BAR

N. D. CARANICOLAS* and N. J. PAPADOPOULOS

*Department of Physics, Section of Astrophysics, Astronomy and Mechanics,
University of Thessaloniki, 540 06 Thessaloniki, Greece*

(Received 14 January 2004)

We study the global and local motion in a barred galaxy model with a massive nucleus. The local model is made up of a two-dimensional perturbed harmonic oscillator and can be derived by expanding the global model in the vicinity of a stable Lagrange point. Low- and high-energy stars in the global model display chaotic motion. Comparison with previous work shows that, for the chaotic motion of low-energy stars, the massive nucleus is responsible. In the local motion, low-energy stars show resonance phenomena while the chaotic phenomena, if any, are negligible. On the other hand, the high-energy stars do not show bounded motion in the local model. This is an indication of particular activity near the centre of galaxies with massive nuclei.

Keywords: Order; Chaos; Low-energy stars; High-energy stars; Barred galaxy

1 INTRODUCTION

In an earlier paper (Caranicolas, 2002) (hereafter called paper P1) we have studied connections between global and local parameters in a barred galaxy model. In the present paper we add to that potential a spherically symmetric nucleus and the total potential becomes

$$\Phi(r, \phi) = -\frac{M_d}{(r^2 + \alpha^2)^{1/2}} - \frac{M_b}{\{r^2[1 + (b^2 - 1)\sin^2 \phi] + c_b^2\}^{1/2}} - \frac{M_n}{(r^2 + c_n^2)^{1/2}}, \quad (1)$$

where r, ϕ are polar coordinates. Equation (1) describes motion in a barred galaxy with a massive nucleus (see below). Here M_d, M_b and M_n are the masses of the disc, bar and nucleus while α, c_b and c_n represent the scale lengths of the disc, bar and nucleus respectively. $b > 1$ stands for the strength of the bar. We use a system of galactic units where the unit of length is 1 kpc, the unit of time is 0.97746×10^8 year and the unit of mass is $2.325 \times 10^7 M_\odot$. The velocity and the angular velocity units are 10 km s^{-1} and $10 \text{ km s}^{-1} \text{ kpc}^{-1}$ respectively while G is equal to unity. Our test particle is a star of mass 1. Therefore, the energy unit (per unit mass) is $100 \text{ km}^2 \text{ s}^{-2}$. In these units the values of the parameters are $\alpha = 12 \text{ kpc}$, $b = 2 \text{ kpc}$, $c_b = 1.5 \text{ kpc}$, $M_d = 9500$, $M_b = 3000$ and $M_n = 400$.

* Corresponding author. E-mail: caranic@astro.auth.gr

As in paper P1, we consider the case where the bar rotates clockwise at a constant angular velocity, Ω_b . The corresponding Hamiltonian, which is known as the Jacobi integral, in rectangular Cartesian coordinates x and y , is

$$\begin{aligned} H_J &= \frac{1}{2}(p_x^2 + p_y^2) + \Phi(x, y) - \frac{1}{2}\Omega_b^2(x^2 + y^2) \\ &= \frac{1}{2}(p_x^2 + p_y^2) + \Phi_{\text{eff}}(x, y) \\ &= E_J, \end{aligned} \quad (2)$$

where p_x and p_y are the momenta, per unit mass, conjugate to x and y ,

$$\begin{aligned} \Phi_{\text{eff}}(x, y) &= -\frac{M_d}{(x^2 + y^2 + \alpha^2)^{1/2}} - \frac{M_b}{(x^2 + b^2y^2 + c_b^2)^{1/2}} \\ &\quad - \frac{M_n}{(x^2 + y^2 + c_n^2)^{1/2}} - \frac{1}{2}\Omega_b^2(x^2 + y^2), \end{aligned} \quad (3)$$

is the effective potential and E_J is the numerical value of the Jacobi integral. If we expand the effective potential (3) in a Taylor series near the centre, we shall find a potential describing local motion.

The motivation for the present work is, firstly, to study the properties of global and local motion in the corresponding potentials and, secondly, to compare the results with those obtained in paper P1 where we had only the bar while the massive nucleus was absent.

In Section 2 we study the properties of orbits in the global model. The local potential, the connection between the local and global parameters and the properties of the local motion are presented in Section 3. We close with a discussion and the conclusions of this work, which are given in Section 4.

2 PROPERTIES OF ORBITS IN THE GLOBAL MODEL

The contours of the constant effective potential (3) are shown in Figure 1. The value of Ω_b is 1.25 in the above-mentioned galactic units. This corresponds to $12.5 \text{ km s}^{-1} \text{ kpc}^{-1}$. There are five stationary points, labelled L_1 to L_5 , at which

$$\frac{\partial \Phi_{\text{eff}}}{\partial x} = 0, \quad \frac{\partial \Phi_{\text{eff}}}{\partial y} = 0. \quad (4)$$

These points are called Lagrange points. The central stationary point L_1 is a minimum of Φ_{eff} . At the other four points L_2 , L_3 , L_4 and L_5 it is possible for the test particle to travel in a circular orbit while appearing to be stationary in the rotating frame. For this orbit the centrifugal and gravitational force precisely balance. The points L_2 and L_3 are saddle points while L_4 and L_5 are maxima of the effective potential. The annulus bounded by the circles through L_2 and L_3 and through L_4 and L_5 is known as the region of corotation.

Our study is based on the numerical integration of the equations of motion

$$\ddot{x} = -2\Omega_b \dot{y} - \frac{\partial \Phi_{\text{eff}}}{\partial x}, \quad \ddot{y} = 2\Omega_b \dot{x} - \frac{\partial \Phi_{\text{eff}}}{\partial y}, \quad (5)$$

where the dot indicates derivative with respect to the time. We use the classical method of the x - p_x ($y = 0$, $p_y > 0$) Poincaré phase plane. Figure 2 shows the structure of this plane for the

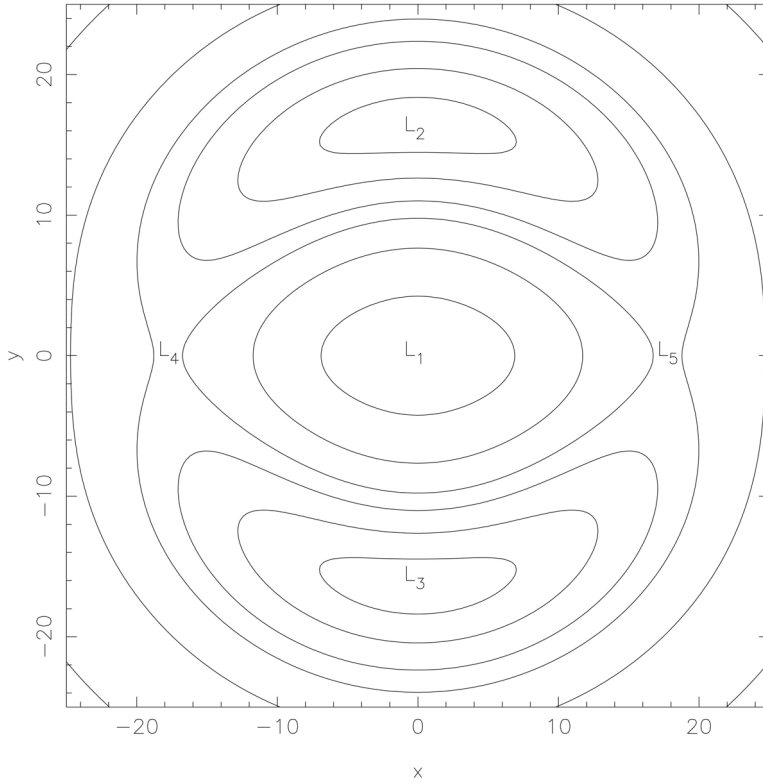


FIGURE 1 Contours of the constant effective potential (3) when $c_b = 1.25$. The values of the parameters are $\alpha = 12$ kpc, $b = 2$ kpc, $c_b = 1.5$ kpc, $c_n = 0.25$ kpc, $M_d = 9500$, $M_b = 3000$ and $M_n = 400$. There are five stationary points labelled L_1 to L_5 .

global Hamiltonian (2) when $E_J = -1000$. There are regular orbits, forming the ‘central set’ of invariant curves as well as a triple set of islands. Furthermore, one can see several sets of smaller secondary islands belonging to orbits starting near periodic orbits of higher resonance. In addition to the regular region, there is a large chaotic sea formed by the chaotic orbits. It is important to note here that this chaotic sea is obviously larger than that observed in the case in paper P1 where the massive nucleus was absent. Also note that the presence of a nucleus gives rise to a large number of secondary islands. The outermost curve is the limiting curve defined by the equation

$$\frac{1}{2}p_x^2 + \Phi_{\text{eff}}(x) = E_J. \quad (6)$$

Figures 3(a)–(d) show four typical orbits. The orbits shown in Figure 3(a) produce one of the central invariant curves. This orbit is a quasiperiodic orbit starting near the stable retrograde periodic orbit which is nearly circular. Such orbits support the disc. The orbit shown in Figure 3(b) produces the set of three outer islands. This orbit belongs to a family of elongated orbits that support the bar. The orbit shown in Figure 3(c) produces two of the three elongated islands embedded in the chaotic sea, while the orbit given in Figure 3(d) is a chaotic orbit. It is evident that the two last types of orbit support both the bar and the disc.

Let us now proceed to see the behaviour of orbits, in the global model, near the centre, that is close to the nuclear region. Figure 4 shows the x – p_x phase plane when $E_J = -2900$. One observes regions of regular motion and chaotic regions as well. In fact, there are

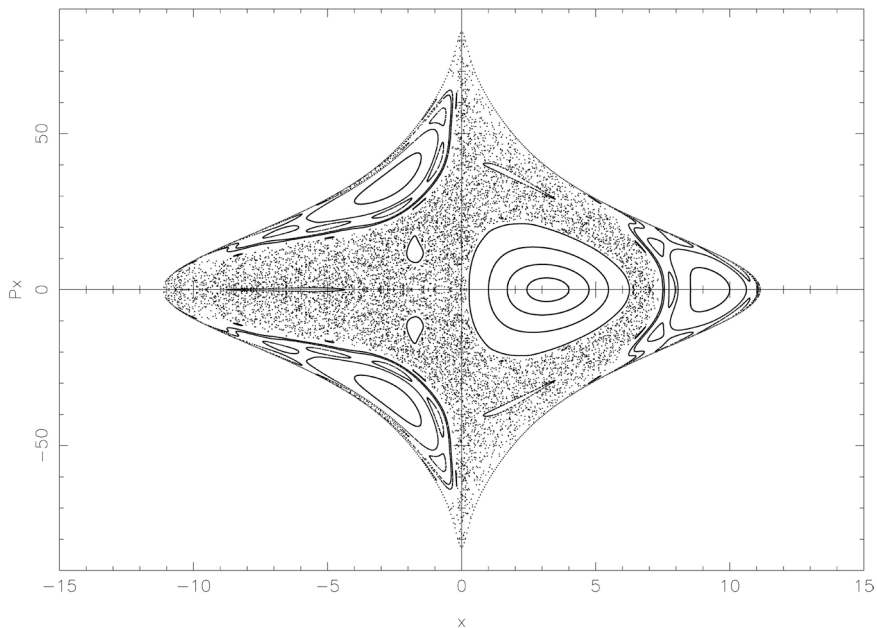


FIGURE 2 The x - p_x phase plane for the global Hamiltonian (2) when $E_1 = -980$. The values of the parameters are as in Figure 1.

two main regular regions consisting of invariant curves that are topologically circles closing around the two invariant points. Those two stable invariant points belong to the two main periodic orbits: the retrograde on the right, and the direct on the left. These periodic orbits are characteristics of the 1:1 resonance and are similar to ellipses around the origin. The rest of the regular region consists of smaller islands produced by quasiperiodic

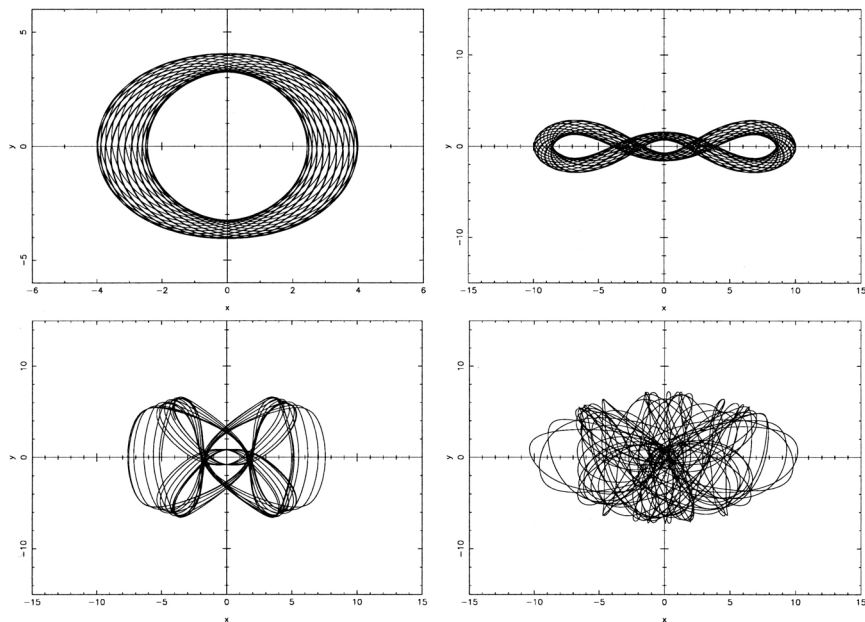


FIGURE 3 (a)–(d) Orbits in the global Hamiltonian (2). The values of parameters are as in Figure 2.

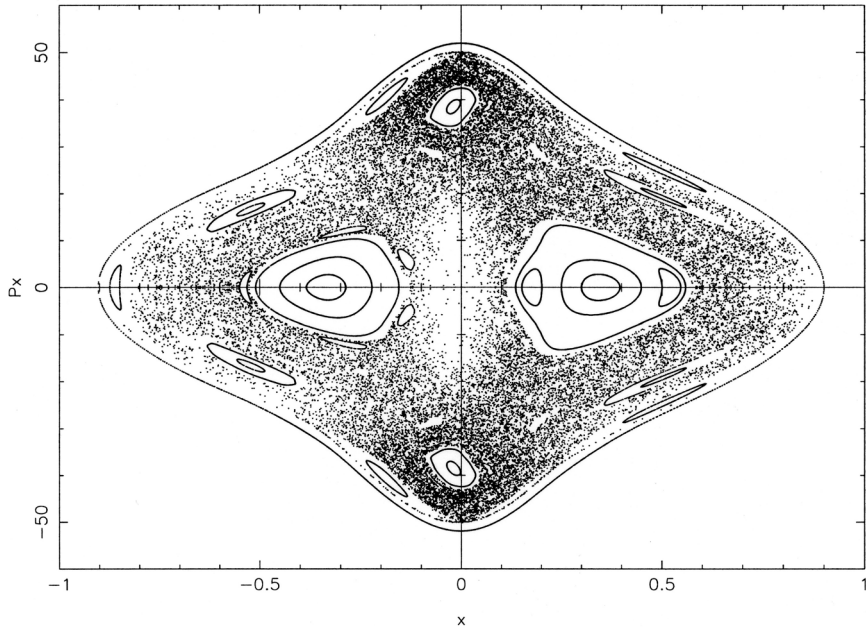


FIGURE 4 Same as Figure 2 when $E_J = -2900$.

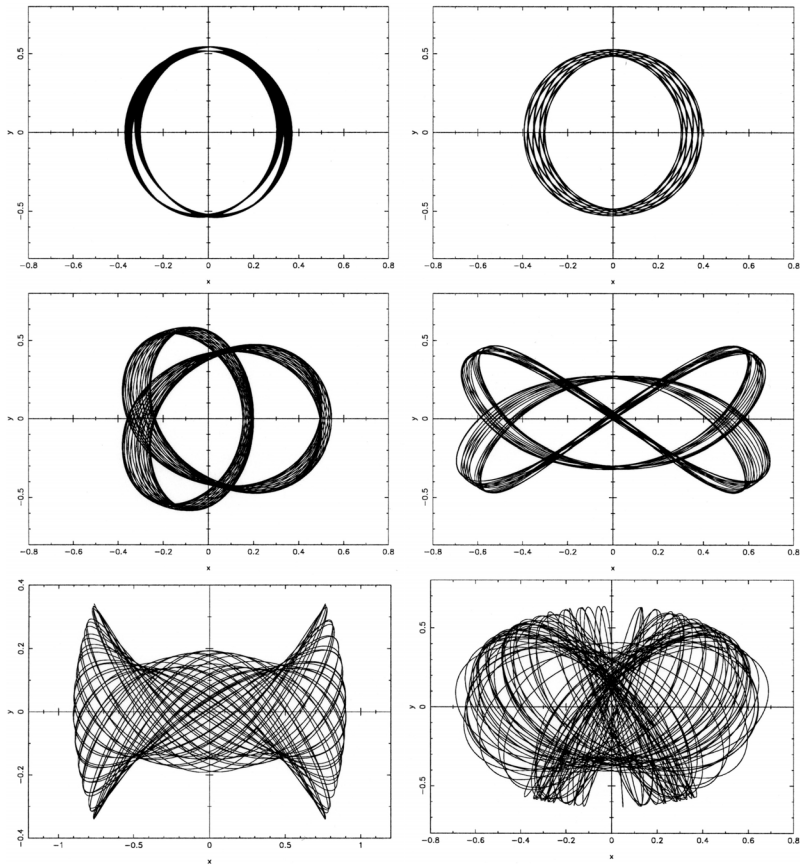


FIGURE 5 (a)–(f) Orbits in the global Hamiltonian (2) when $E_J = -2900$.

orbits belonging to higher resonances. The chaotic region consists of a large chaotic sea with several sticky regions. It is well known that the phenomenon of stickiness is common in barred galaxy models (Caranicolas and Karanis, 1998; Karanis and Caranicolas, 2002).

Comparing the present results with those given in paper P1 we see that the presence of the massive nucleus changes dramatically the properties of motion in our barred galaxy model. There we had only regular motion; strictly speaking, there were only box orbits forming regular invariant curves while, in the present case, we have resonant periodic or quasiperiodic orbits producing large or small islands. Furthermore the larger parts of orbits are chaotic. We return to this point in the discussion.

In order to visualize the structure of motion near the nuclear region we present six typical orbits which are shown in Figures 5(a)–(f). Figures 5(a) and (b) show two orbits starting near the starting points of direct and the retrograde stable periodic orbits. Each of those orbits produces one invariant curve belonging to the main set of invariant curves and closing around one of the fixed invariant points on the left- or the right-hand side respectively in Figure 4. The orbit shown in Figure 5(c) produces the set of the two small islands embedded inside the main set of invariant curves on the right-hand part of Figure 4 while the orbit shown in Figure 5(d) produces one of the islands that intersects the p_x axis. Finally Figure 5(e) shows a box orbit producing the outer invariant curve in Figure 4 while the orbit shown in Figure 5(f) is a chaotic orbit.

3 MOTION IN THE LOCAL POTENTIAL

Expanding the effective potential (3) in a McLaurin series near the stable Lagrange point L_1 , we obtain the local effective potential which is

$$\begin{aligned}
 U_{\text{eff}}(\Delta x, \Delta y) &= U_{\text{eff}}(0, 0) + \frac{1}{2}A(\Delta x)^2 + \frac{1}{2}B(\Delta y)^2 \\
 &\quad - \frac{3}{8}[\alpha_1(\Delta x)^4 + 2\alpha_2(\Delta x)^2(\Delta y)^2 + \alpha_3(\Delta y)^4] \\
 &\quad - \frac{1}{2}\Omega_0^2[(\Delta x)^2 + (\Delta y)^2], \tag{7}
 \end{aligned}$$

where we have set

$$U_{\text{eff}} = \frac{\alpha}{M_d} c_n^2 \Phi_{\text{eff}}, \tag{8}$$

in order to avoid large numbers. Writing, for convenience, $x = \Delta x$, $y = \Delta y$, $V_{\text{eff}} = U_{\text{eff}}(x, y) - U_{\text{eff}}(0, 0)$, equation (7) becomes

$$V_{\text{eff}} = \frac{1}{2}Ax^2 + \frac{1}{2}By^2 - \frac{3}{8}(\alpha_1 x^4 + 2\alpha_2 x^2 y^2 + \alpha_3 y^4) - \frac{1}{2}\Omega_0^2(x^2 + y^2), \tag{9}$$

where

$$\begin{aligned}
 A &= \frac{c_n^2}{\alpha^2} + \frac{\alpha c_n^2 M_b}{M_d c_b^3} + \frac{\alpha M_n}{M_d c_n}, \\
 B &= \frac{c_n^2}{\alpha^2} + \frac{\alpha b^2 c_n^2 M_b}{M_d c_b^3} + \frac{\alpha M_n}{M_d c_n},
 \end{aligned}$$

$$\begin{aligned}
 \alpha_1 &= \frac{1}{\alpha^4} + \frac{\alpha M_b}{M_d c_b^5} + \frac{\alpha M_n}{M_d c_n^3}, \\
 \alpha_2 &= \frac{c_n^2}{\alpha^4} + \frac{\alpha b^2 c_n^2 M_b}{M_d c_b^5} + \frac{\alpha M_n}{M_d c_n^3}, \\
 \alpha_3 &= \frac{c_n^2}{\alpha^4} + \frac{\alpha b^4 c_n^2 M_b}{M_d c_b^5} + \frac{\alpha M_n}{M_d c_n^3}, \\
 \Omega_0^2 &= \frac{\alpha c_n^2 \Omega_b^2}{M_d}.
 \end{aligned}
 \tag{10}$$

As one can see, from equations (10), the coefficients of the local effective potential are functions of the physical quantities entering the global effective potential.

The local Hamiltonian is

$$H_L = \frac{1}{2}(X^2 + Y^2) + V_{\text{eff}}(x, y) = h_L,
 \tag{11}$$

where X and Y are the local momenta, per unit mass, conjugate to x and y while h_L is the numerical value of the local energy.

In order to connect the global energy E_J to the local energy h_L we proceed as follows. The equation $E_{J0} = \Phi_{\text{eff}}(0, 0)$ defines a point in the (x, y) plane while $E_J = \Phi_{\text{eff}}(x, y)$ defines a curve in the same plane. The global motion takes place inside this curve which is known as the zero-velocity curve. On the other hand, $h_L = V_{\text{eff}}(x, y)$ defines a curve in the (x, y) plane inside which the local motion takes place. This curve is the local zero-velocity curve. We consider only bounded motion; that is, the zero-velocity curves are always closed curves. The local energy h_L is connected to the global energy through the relation

$$\begin{aligned}
 h_L &= U_{\text{eff}}(x, y) - U_{\text{eff}}(0, 0) \\
 &= \frac{\alpha c_n^2}{M_d} [\Phi_{\text{eff}}(x, y) - \Phi_{\text{eff}}(0, 0)] \\
 &= \frac{\alpha c_n^2}{M_d} (E_J - E_{J0}).
 \end{aligned}
 \tag{12}$$

Let us now study the properties of local motion. For the adopted values of the global parameters and $\Omega_b = 1.25$ we find that $A = 2.1$, $B = 2.3$, $\alpha_1 = 32.4$, $\alpha_2 = 32.5$, $\alpha_3 = 32.8$ and $\Omega_0 = 0.011$. For the value of global energy $E_J = -2900$ we find that, using equation (12), $h_L = 0.11776$. It is amazing that this value of local energy is much larger than the energy of escape for the corresponding local potential (Caranicolas and Karanis, 1998), which is given by

$$h_{\text{esc}} = \frac{(B - \Omega_0^2)^2}{6\alpha_1}.
 \tag{13}$$

For the above values of the parameters, equation (13) gives $h_{\text{esc}} = 0.022522$. This value is less than $h_L/5$. Therefore, one concludes that near the nucleus we do not have local motion or what are equivalent local orbits escape the nuclear region because they possess a high local energy. In order to obtain an idea of the local motion near the nucleus, one must go to very low energies, that is $h \ll h_L$.

Figure 6 shows the x - X ($y = 0, Y > 0$) Poincaré phase plane for the local motion when $h = 0.0225$. The motion is regular, and the phase plane has all the characteristics of the 1:1

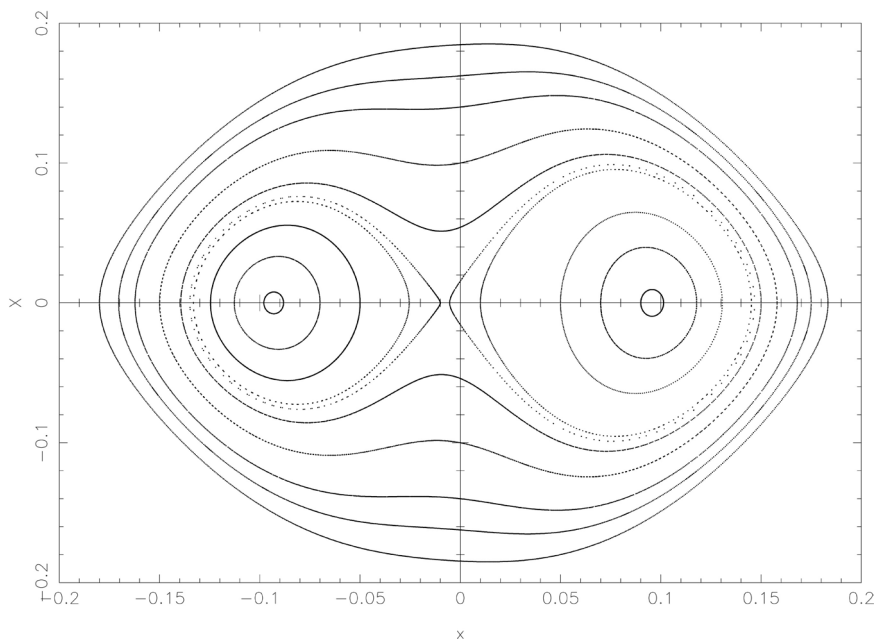


FIGURE 6 The x - X phase plane for the local Hamiltonian (11) when $h = h_L = 0.0225$.

resonance. There are two stable periodic points corresponding to the direct and the retrograde resonant periodic orbits respectively. The unstable periodic point gives an orbit which, in the absence of rotation, is the y axis. Thus, one concludes that local motion near the nucleus consists of a low-energy 1:1 resonant periodic orbit; chaotic phenomena, if any, are negligible.

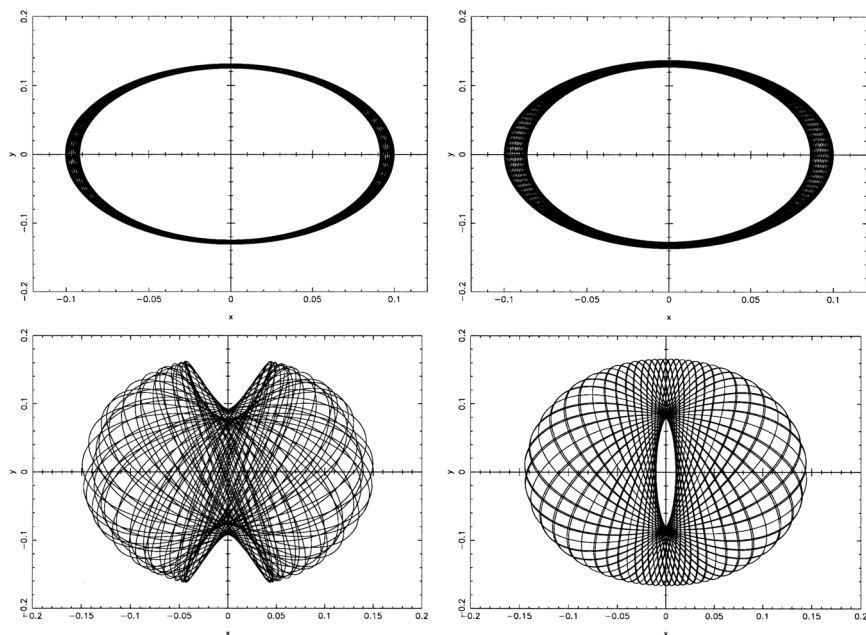


FIGURE 7 (a)–(d) Orbits in the global Hamiltonian (11) when $h = 0.0225$.

This situation is completely different from that displayed in paper P1 where the nucleus was not present. There, all orbits in the local potential were box orbits without any resonance phenomena.

Figures 7(a)–(d) show four orbits for the local Hamiltonian (11). Figure 7(a) and (b) show two quasiperiodic orbits starting near the retrograde and direct periodic points respectively. Figure 7(c) shows an orbit starting near the unstable periodic point while the orbit shown in Figure 7(d) is a box orbit and produces one of the outer invariant curves shown in Figure 6.

4 DISCUSSION

One of the most important approaches for understanding the dynamic behaviour of a galactic dynamic model is based on the knowledge of the chaotic versus ordered nature of its orbits. In the present work we tried to achieve this with a global and local potential describing a barred galaxy with a massive nucleus. The corresponding local potential was found by expanding the global model in a McLaurin series around a stable Lagrange point which coincides with the origin. This local potential is a potential made up of a two-dimensional perturbed harmonic oscillator. The study of motion in those potentials has been an active field of research in the last decades (see for example Saito and Ichimura (1979), Caranicolas (1984, 1994, 2000), Innanen (1985) and Caranicolas and Karanis (1999)). In the last few years the study of the properties of motion in those systems has been made using precise and modern analytical (Elife, 1999, 2001; Elife and Deprit, 1999) or numerical (Lara *et al.*, 1999; Karanis and Caranicolas, 2002) tools.

As expected, the local parameters and the corresponding local energy are functions of the global parameters and the global energy. Our numerical experiments in the global model, for high energies, suggest that more than 50% of orbits are chaotic. Comparing this outcome with those of paper P1 we see that, in the present case, we have a sharp increase in the chaotic orbits. It is evident that the massive nucleus is responsible for this phenomenon. It is easy to see that the chaotic region in Figure 2 is very much extended. This means that the nucleus affects not only the region near the centre but also areas far from that. Another interesting observation is that the presence of massive nucleus does not seem to affect the figure-of-eight quasiperiodic orbits which are building blocks of the barred structure of the galaxy. This result agrees with recent observations made by the Hubble Space Telescope which showed that a number of Seyfert galaxies display strong nuclear bars (Regan and Mulchaey, 1999).

On the other hand, the global motion near the nucleus has the characteristic of 1:1 resonance. Furthermore the chaotic sea seems to be larger than that observed in Figure 2. This is natural because of the presence of the nearby massive nucleus. The above results are completely different from the corresponding results in paper P1, where the motion was regular and where all orbits for the global motion near the centre were box orbits.

In order to estimate better the degree of chaos displayed by the orbits in Figures 2 and 4 we decided to compute the maximal Lyapunov characteristic number (LCN) (for details see Lichtenberg and Lieberman (1983)). The results are shown in Figure 8. The dotted curve shows the LCN for a chaotic orbit with initial conditions in a chaotic sea in Figure 2 while the solid curve is the LCN for a chaotic orbit with initial conditions in the chaotic sea of Figure 4. The LCN represented by the solid curve is about ten times the LCN indicated by the dotted curve. Therefore, one can say that in this case we have not only fast chaos (Caranicolas and Vozikis, 1987) where the LCN is of the order of unity but very fast chaos where the LCN is about three times larger. It is evident that this is an indication of strong activity in the nuclear region.

Let us now consider the local motion. The local potential (9) has characteristics of the 1:1 resonance. Such potentials are known as perturbed elliptic oscillators (Deprit, 1991).

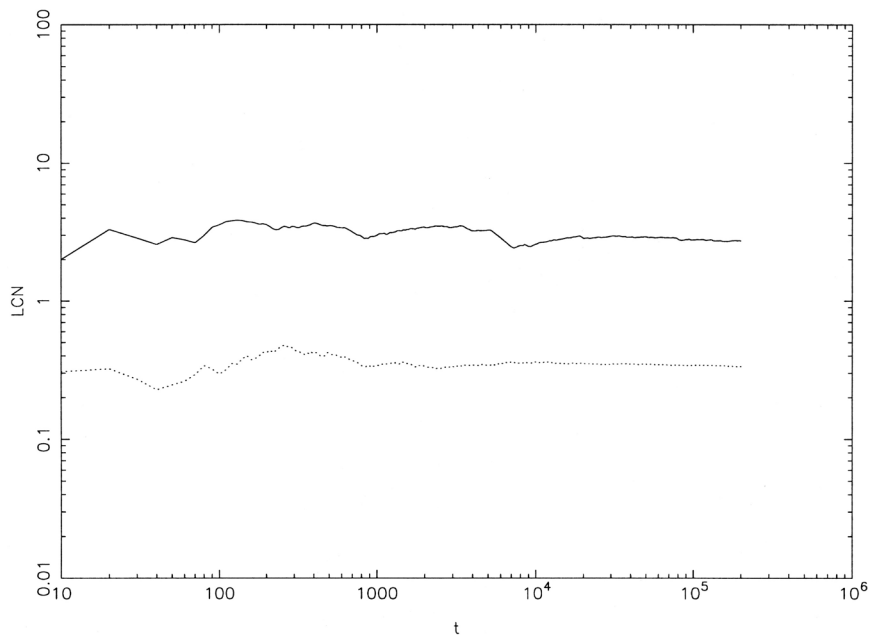


FIGURE 8 LCNs for the two chaotic orbits. (.....), LCN for an orbit in the chaotic sea of Figure 2; (—), LCN for an orbit in the chaotic sea of Figure 4.

It is interesting that for the corresponding local energy given by equation (12) the local motion is not bounded. In order to obtain bounded local motion, one must go to very low local energies. Strictly speaking, the presence of the massive nucleus makes the local energy increase dramatically, so that considering all the local zero-velocity curves results in unbounded local motion. For local energies slightly lower than the energy of escape we observe resonance phenomena, namely the 1:1 resonant periodic orbits. Extensive numerical calculations in the local potential suggest that chaotic phenomena, if any, are negligible.

Bearing all the above in mind we can say that this situation is completely different from that observed in paper P1 where the properties of local motion were the same as those of the global motion near the centre (see Figures 4 and 5 in paper P1). Here the corresponding local motion does not appear to exist, and only very-low-energy local motion seems to be present. Furthermore, the fact that the corresponding LCN, which was computed in the chaotic sea near the nuclear region, is much more than unity suggests that there is particular activity in the motion in the central parts of galaxies with strong nuclear bars.

References

- Caranicolas, N. D. (1984) *Celestial Mech.* **33**, 209.
- Caranicolas, N. D. (1994) *Astron. Astrophys.* **287**, 752.
- Caranicolas, N. D. (2000) *New Astron.* **5**, 397.
- Caranicolas, N. D. (2002) *J. Astron. Astrophys.* **23**, 173.
- Caranicolas, N. D., and Karanis, G. I. (1998) *Astrophys. Space Sci.* **259**, 45.
- Caranicolas, N. D., and Karanis, G. I., (1999) *Astron. Astrophys.* **342**, 389.
- Caranicolas, N. D., and Vozikis, Ch. (1987) *Celestial Mech.* **40**, 35.
- Deprit, A. (1991) *Celestial Mech.* **51**, 202, 635.
- Carlberg, R. G., and Innanen, K. A. (1987) *Astron. J.* **94**, 666.
- Elipe, A. (1999) *Phys. Rev. E*, **61**.
- Elipe, A. (2001) *Math. Comput. Simulation* **57**, 217.

- Elife, A., and Deprit, A. (1999) *Mech. Res. Commun.* **26**, 635.
- Innanen, K. A. (1985) *Astron. J.* **90**, 2377.
- Karanis, G. I., and Caranicolas, N. D. (2002) *Astron. Nach.* **323**, 1.
- Lara, M., Elife, A., and Palacios, M. (1999) *Math. Comput. Simulation* **49**, 351.
- Lichtenberg, A. J., and Lieberman, M. A. (1983) *Regular and Stochastic Motion*, Springer, Berlin.
- Regan, W. M., and Mulchaey, J. S. (1999) *Astrophys. J.* **526**, 665.
- Saito, N., and Ichimura, A. (1979) In: Casati, G. and Ford, J. (eds.), *Stochastic Behavior in Classical and Quantum Hamiltonian Systems*, Springer, Berlin, p. 137.